2.3. Equipment.

A flowsheet of the equipment is given in Fig. 2.5. All the experiments were carried out in a vertical, cylindrical vessel of perspex (A) with an inside diameter of 29 cm and an outside diameter of 30 cm. The height of the column was 4 m.

In general it is assumed that with a column of these dimensions the information obtained is representative of a large-scale industrial bubble column.

Air was supplied by a compressor (B). In order to control the gas flow rate, part of the gas flow could be blown off.

To obtain air with an oil content of less than 0.01 ppm, a filter set (C) was installed to separate possible traces of oil. The gas flow rate was measured by means of a rotameter (D). At the outlet of the rotameters, pressure and temperature of the gas flow were measured (E).

As standard temperature and pressure we used 20 °C and 1 bar respectively. Furthermore, the gas flow was cooled off and saturated with water vapour in a spray-tower (F) packed with Raschig rings. After passing a cyclone (G) to separate possible droplets of water, air was led into the column through the gas distributor (H).

The gas distributor used (diameter 28 cm) was of the spider-type with six radial branches. The sparger was located about 18 cm above the bottom of the vessel. The air was fed through 60 orifices of 1.9 mm diameter each. These were directed downwards at an angle of 45 ° with the vertical axis and were distributed at

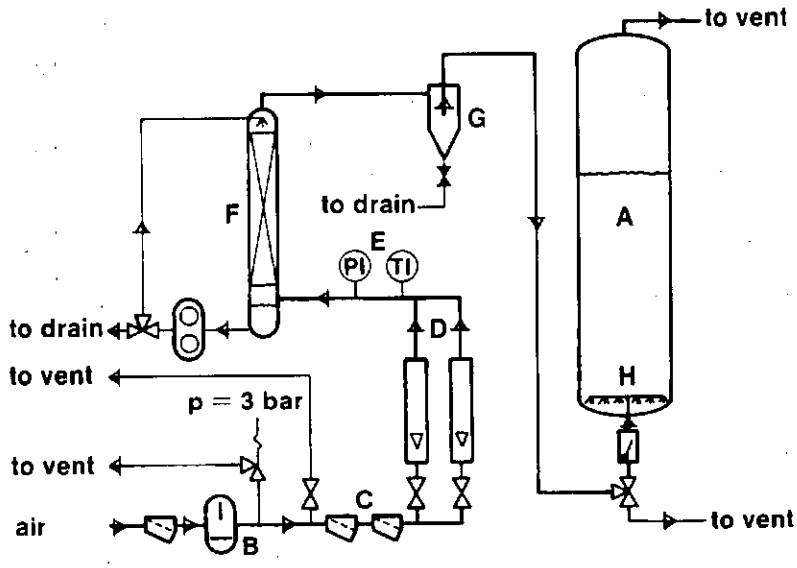

Fig. 2.5. Equipment used for the investigation of the hydrodynamic behaviour of a gas-liquid-solid dispersion in a column. Height 4 m; inside diameter 0.29 m; height of gas sparger 0.18 m; sparger diameter 0.28 m.

equal distances along each branch.
Van Dierendonck et al. [10] found that the bubble diameter is independent of the diameter of the orifices if the gas velocity in the orifices is higher than a critical velocity:

$$v_{or} > C_8 \, d_o^{-1.65} \qquad (2\text{-}77)$$

where:

$$C_8 = 5.3 \; 10^5 \; m^{2.65} \; s^{-1} \qquad (2\text{-}78)$$

For an orifice diameter of 1.9 mm this inequality results in:

$$u_G > 5 \; 10^{-3} \; m \; s^{-1} \qquad (2\text{-}79)$$

In this work, the superficial gas velocity always satisfied eqn (2-79).
To assure uniform bubbling of gas across the entire gas disperser, the pressure drop across the orifice must be so high that changes of the static pressure owing to fluctuations of the height of the dispersion will not influence this uniformity. Measurement of the pressure drop across the orifice and of the fluctuations of the dispersion taught us that uniform distribution of gas was ensured.

2.4. Physical properties.

Although there is no consensus about the effect of the nature of the gas on the behaviour of the dispersion [43,54,70,71], we used air only as the dispersed gas phase for the sake of simplicity and safety.
The system consisted of demineralized water or an electrolyte solution, with or without solid particles. For the demineralized water system, we applied H_0/T values of 2.6, 6.0 and 8.6.
Experiments with solid particles in the demineralized water/air system were performed with a H_0/T value of 6.2 and solids concentrations of 4, 8 and 12 kg m^{-3}.
The electrolyte solution was made up of 17 wt % NH_4NO_3 and 23 wt % H_3PO_4.
We investigated the hydrodynamic behaviour of this electrolyte solution at a H_0/T value of 6.1.
Experiments with solid particles in the electrolyte solution were performed with a H_0/T value of 6.2 and solids concentrations of 4 and 8 kg m^{-3}.
As solid phase, we used activated carbon, Eponit 114n from Degussa. By sieving, we obtained a fraction of particles with a diameter of less than 38 μm. This fraction was washed with water, dried, and stored at 120 °C. The cumulative distribution curve of this fraction is given in Fig. 2.6. It shows that about 60 wt % of the particles has a diameter of less than 10 μm. The particle diameter distribution has been determined by means of micro-sieves and a Coulter-Counter. In Table 2.4., a survey of the physical properties of the gas, liquid and solid phase is given.

2.5. Results.

2.5.1. Average gas holdup.

The average gas holdup was calculated according to eqn (2-2). To this end, the height of the clear liquid and that of the dispersion have been determined with a measuring scale on the outside of the column.
The average gas holdup of air in demineralized water was first determined. Clear liquid heights were 0.76, 1.73 and 2.50 m. In Fig. 2.7., the average gas holdup is given as a function of the superficial gas velocity. It can be seen that there is a tendency for ε_{av} to decrease with increasing clear liquid height.

Table 2.4. Physical properties of the gas, liquid and solid phase used in the experiments of the present study at 20 °C.

gas phase:	air	$\eta_G = 1.8\ 10^{-5}$ Pa s $\rho_G = 1.2$ kg m^{-3}
liquid phase:	demineralized water	$\eta_L = 1\ 10^{-3}$ Pa s $\rho_L = 1\ 10^{3}$ kg m^{-3} $\sigma = 72\ 10^{-3}$ N m^{-1}
	electrolyte solution	$\eta_L = 1.9\ 10^{-3}$ Pa s $\rho_L = 1.2\ 10^{3}$ kg m^{-3} $\sigma = 78\ 10^{-3}$ N m^{-1}
solid phase:	activated carbon Eponit 114n Degussa	
		$d_{p_w} = 9.9 \pm 5.3$ µm $d_{p_n} = 4.1 \pm 2.2$ µm

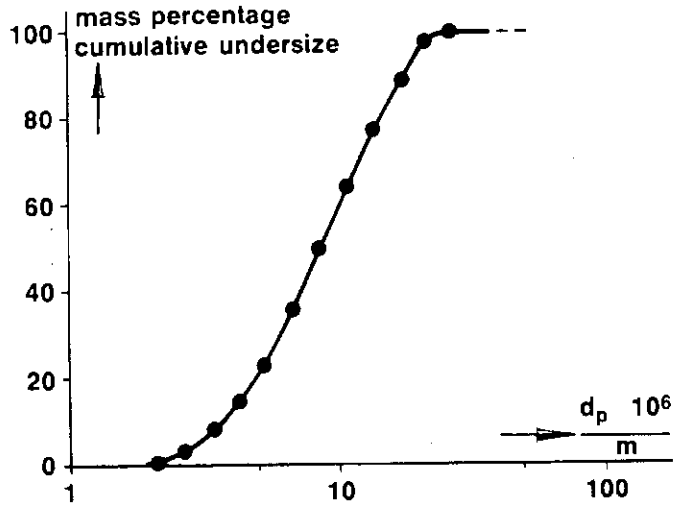

Fig. 2.6. Cumulative undersize distribution of carbon particles as a function of particle diameter.

The data have been correlated by means of eqn (2-6), i.e. the reciprocal values of ε_{av} have been plotted versus u_G. Values of b and v_o are tabulated in Table 2.5., where also the maximum and the mean deviation of the data points from the calculated best-fit values are given.
The values calculated from the five correlations obtained from the literature and mentioned in Table 2.5. are in good agreement with our experimental data. Only the correlation of Akita and Yoshida shows a somewhat larger deviation for smaller clear liquid heights.
In eqn (2-6) the constants b and v_o were obtained after application of a best-fit procedure to our experimental results. Towell et al. and Reith et al. had chosen b = 2 and determined the value of v_o. Hughmark had chosen b = 2 and $v_o = 0.35$ m s^{-1}.

Table 2.5. Best-fit values of b, ε_∞ and v_0 for the system air/demineralized water and comparison of our experimental values of ε_{av} with those predicted by the correlations of Table 2.1.

		This work, eqn (2-6)			
H_0/m	v_0/(m s^{-1})	b	ε_∞	max. dev.	mean dev.
0.76	0.32	2.05	0.49	10 %	3 %
1.73	0.38	2.08	0.48	8 %	1 %
2.50	0.36	2.40	0.42	20 %	3 %

	Van Dierendonck et al, eqn (2-10)		Hughmark, eqn (2-11)		Mersmann, eqn (2-13)	
H_0/m	max. dev.	mean dev.	max. dev.	mean dev.	max. dev.	mean dev.
0.76	22 %	9 %	22 %	6 %	17 %	9 %
1.73*	11 %	13 %	11 %	6 %	17 %	4 %
2.50*	30 %	16 %	16 %	9 %	10 %	4 %

	Towell et al., Reith et al. eqn (2-9)			Yoshida and Akita eqn (2-12)	
H_0/m	v_0/(m s^{-1})	max. dev.	mean dev.	max. dev.	mean dev.
0.76	0.31	10 %	3 %	25 %	17 %
1.73	0.39	8 %	2 %	21 %	6 %
2.50	0.38	20 %	7 %	9 %	3 %

* Van Dierendonck proposed eqn (2-10) for $H_0/T \leq 3$. As a consequence, it is not allowed to apply eqn (2-10) under our experimental conditions.

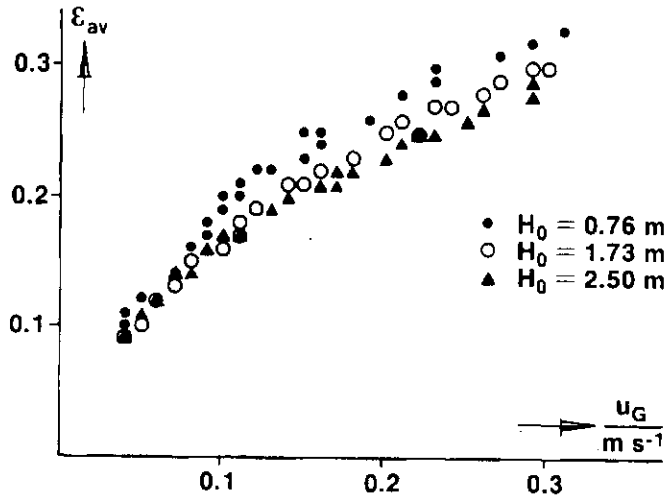

Fig. 2.7. Average gas holdup as a function of superficial gas velocity for the system air/demineralized water for different clear liquid heights.

Further experiments were performed with the electrolyte solution containing 17 wt % NH_4NO_3 and 23 wt % H_3PO_4. The clear liquid height of this electrolyte solution was 1.76 m. In Fig. 2.8., the average gas holdup of this electrolyte

solution and that of the pure solvent are compared. No difference is observed between the values of ε_{av} of the electrolyte solution and those of the pure solvent. In Table 2.6., the values of b and v_o are given as well as the maximum and mean deviation of our experimental results with respect to the values predicted by other investigators.
From Table 2.6. it is clear that all the correlations except that of Van Dierendonck, which was proposed for $H_O/T \leq 3$ only, predict our experimental values very well. Furthermore, it is found that the value of v_o increases when electrolyte is added to a pure solvent.

Table 2.6. Best-fit values of b, ε_∞ and v_o for the system air/electrolyte solution ($H_O/T = 6.1$) and comparison of our experimental values of ε_{av} with those predicted by the correlations of Table 2.1.

	$v_o/(m\ s^{-1})$	b	ε_∞	max. dev.	mean dev.
This work, eqn (2-4)	0.46	1.87	0.53	7 %	2 %
Towell et al., eqn (2-9)					
Reith et al., eqn (2-9)	0.44	2	0.5	5 %	1 %
van Dierendonck et al., eqn (2-10)				37 %*	32 %*
Hughmark, eqn (2-11)				13 %	7 %
Akita and Yoshida, eqn (2-12)				20 %	7 %
Mersmann, eqn (2-13)				14 %	5 %

* Van Dierendonck proposed eqn (2-10) for $H_O/T \leq 3$. As a consequence, it is not allowed to apply eqn (2-10) under the present experimental conditions.

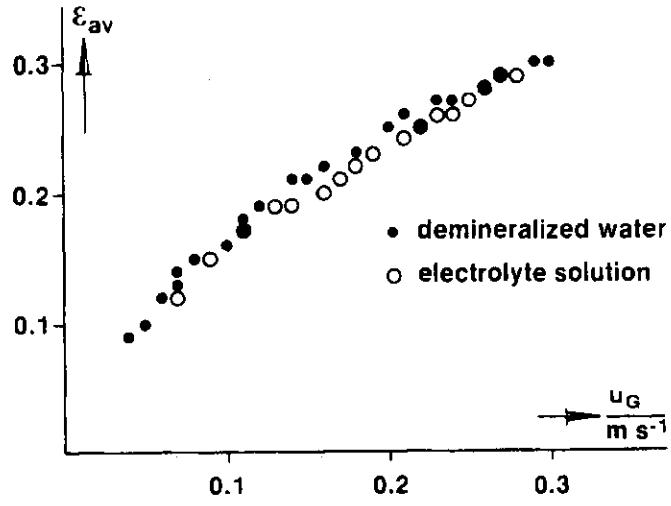

Fig. 2.8. Average gas holdup as a function of superficial gas velocity for the system air/demineralized water and the system air/electrolyte solution, containing 23 wt % H_3PO_4 and 17 wt % NH_4NO_3.($H_O/T = 6.1$)

At a clear liquid height of about 1.80 m, we performed experiments with the system air-demineralized water to which carbon particles were added. For

the solid phase we used Eponit 114n from Degussa at concentrations of 4, 8 and 12 kg m^{-3}.
In Fig. 2.9., the gas holdup of these slurry systems is given as a function of the superficial gas velocity. The figure shows that addition of carbon particles up to a concentration of 12 kg m^{-3} does not influence the value of the average gas holdup with respect to that of the pure solvent.
In Table 2.7., the values of b and v_o are listed. No comparison has been made with other correlations because these are not intended to apply to slurry systems.

Table 2.7. Best-fit values of b, ε_∞ and v_o for the system air/demineralized water/carbon particles.

$\bar{C}_p$/(kg m^{-3})	H_0/m	v_o/(m s^{-1})	b	ε_∞	max. dev.	mean dev.
0	1.73	0.38	2.08	0.48	8 %	1 %
4	1.79	0.34	2.23	0.45	5 %	2 %
8	1.80	0.33	2.26	0.44	11 %	2 %
12	1.80	0.34	2.33	0.43	7 %	2 %

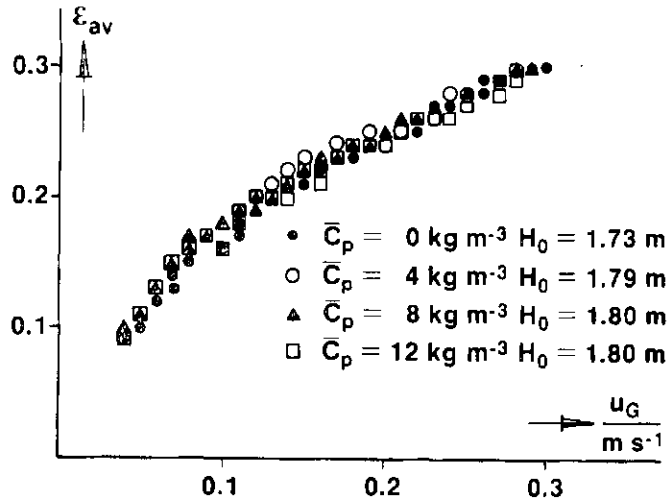

Fig. 2.9. Average gas holdup as a function of superficial gas velocity for the system air/demineralized water/carbon particles for different solids concentrations.

We have seen that with a clear liquid height of about 1.8 m, addition of carbon particles up to a concentration of about 12 kg m^{-3} or addition of electrolyte to the pure solvent does not significantly influence the average gas holdup with respect to that of the pure liquid at the same value of the superficial gas velocity.
However, when adding both carbon particles and electrolyte to the pure solvent, a totally different picture arises. The total height of the dispersion is increased enormously resulting in a value of the average gas holdup of about 0.5. The dispersion height is constant for $u_G > 0.1$ m s^{-1} and the level of the dispersion is flat and fairly quiet.
It appears that the top of the dispersion consists of a foam layer. The height

of the dispersion without foam is measured with a float.
As is seen from Fig. 2.10., the average gas holdup of the dispersion without foam increases continuously and its value is larger than that for the other investigated systems at the same value of the superficial gas velocity. The average gas holdup of the foamless part of the dispersion has been calculated from:

$$\varepsilon_{av} = (H_F - H_0)/H_F \qquad (2\text{-}80)$$

where H_F is the height of the float above the bottom of the column.
The experiments were carried out at clear liquid heights of 1.79 and 1.83 m with carbon particle concentrations of 4 and 8 kg m^{-3} respectively. Fig. 2.10. shows that an increase of the particle concentration does not influence the average gas holdup.
The values of v_o and b were determined by plotting the reciprocal values of ε_{av} of the foamless part of the dispersion against $1/u_G$.
It is evident that the total average gas holdup (including foam) for $u_G > 0.1$ m s^{-1} is given by:

$$\varepsilon_{av} = 0.5 \qquad (2\text{-}81)$$

Values of b, ε_∞ and v_o for the foamless part of the dispersion are given in Table 2.8.

Table 2.8. Best-fit values of b, ε_∞ and v_o for the foamless part of the system air/electrolyte solution/carbon particles.

$\bar{C}_p$/(kg m^{-3})	H_0/m	v_o/(m s^{-1})	b	ε_∞	max. dev.	mean dev.
4	1.79	0.35	1.02	0.98	13 %	4 %
8	1.83	0.32	1.17	0.85	7 %	3 %

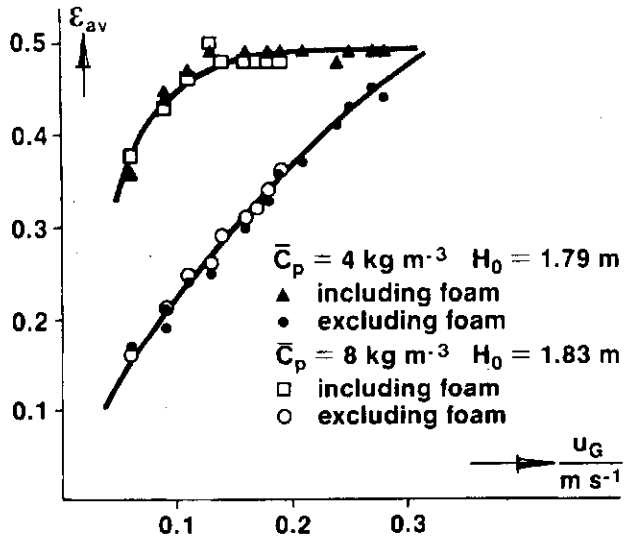

Fig. 2.10. Average gas holdup as a function of the superficial gas velocity for the system air/electrolyte solution, containing 23 wt % H_3PO_4 and 17 wt % NH_4NO_3/carbon particles.

The values of b presented in Table 2.8. satisfy the requirement that $b > 1$ i.e. $\varepsilon_\infty < 1$.
It is interesting to note that the height of the foam layer has a maximum value at a superficical gas velocity of about 0.15 m s^{-1} as is shown in Fig. 2.11. The decrease of the foam height for $u_G > 0.15$ m s^{-1} is due to the more intimate mixing between foam layer and dispersion caused by, in particular, large bubbles. This behaviour of the foam layer was also reported by De Rooy et al. [11].

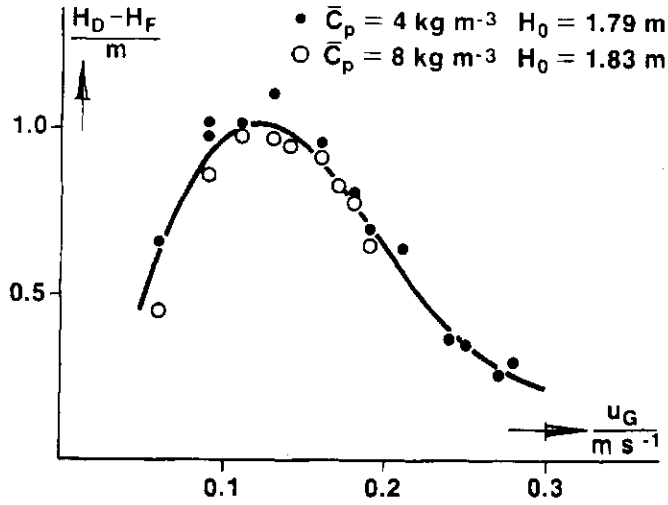

Fig. 2.11. Height of foam layer as a function of the superficial gas velocity for two different concentrations of solid particles.

2.5.2. Gas-holdup distribution.
At seven heights along the column, provisions were made to determine the local gas holdup of the dispersion at various radial positions. Pressure was measured at 7, 27, 51, 80, 109, 138 and 167 cm from the bottom.
We used glass tubes which had a sliding fit in a hole in the wall of the column. Inside the column the tube was provided with a 0.5 mm diameter capillary tube which could be closed by means of a stopcock at the outerside of the column. The glass tubes were connected to manometer tubes by flexible tubings.
Before each experiment, the manometer tubes were filled with the same liquid as was used in the column. When the stopcocks were opened, liquid from the manometer tubes slowly flowed into the column, preventing air bubbles from entering the manometer tubes. The difference between the manometer levels of two successive pressure points was measured. These experiments were performed at radial distances of 2.5, 4.5, 9.5 and 14.5 cm from the axis of the column. From Fig. 2.12., it can be deduced that:

$$\varepsilon_{n,n+1} = h_{n,n+1}/z_{n,n+1} \qquad (2\text{-}82)$$

for $n = 1,\ldots,6$ and that:

$$\varepsilon_{0,1} = 1 - h_{0,1}/(H_D - h_1) \qquad (2\text{-}83)$$

with $h_1 = 1.67$ m.

The average gas holdup for a cross-sectional area of the column was calculated from:

$$\epsilon(z) = (1/(\pi R^2)) \int_0^R \epsilon(r,z)\, r\, dr \qquad (2\text{-}84)$$

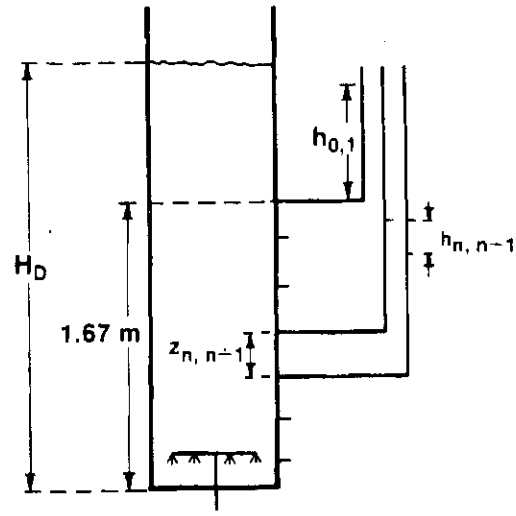

Fig. 2.12. Equipment used for the measurement of gas holdup distribution.

The measurements were performed with three different clear liquid heights, viz. 0.75, 1.80 and 2.50 m.
In Figs. 2.13., 2.14 and 2.15, the axial gas holdup distribution in the system air/demineralized water is given for these clear liquid heights and for three different values of the superficial gas velocity. The average values of the gas holdup are represented by the dotted lines.
For all clear liquid heights, it may be concluded that:
- at the top of the dispersion the gas holdup is relatively large (foam);
- near the sparger, the gas holdup is relatively small;
- calculation of the average values of the gas holdup from the local values by means of eqn (2-15) gives the same values of the average gas holdup as found by means of eqn (2-2);
- for the middle section, the value of the gas holdup is lower than the average value.

Under identical conditions, experiments were performed with a slurry consisting of carbon particles with concentrations of 4, 8 and 12 kg m^{-3} and demineralized water.
No difference was found between the values of the local gas holdup of the system air/demineralized water with and without carbon particles. Addition of carbon particles to demineralized water did not change the value of the local gas holdup at identical heights.
In Fig. 2.16., the axial gas holdup distribution has been given for a dispersion of 4 kg m^{-3} carbon particles in water for three different values of the superficial gas velocity. The gas holdup distribution is almost identical with that of the air/water system.

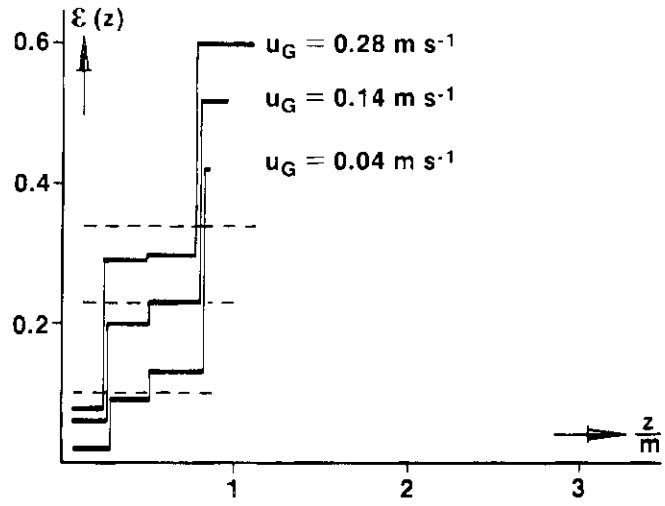

Fig. 2.13. Axial gas holdup distribution for the system air/demineralized water, with H_0 = 0.75 m, for three different superficial gas velocities.

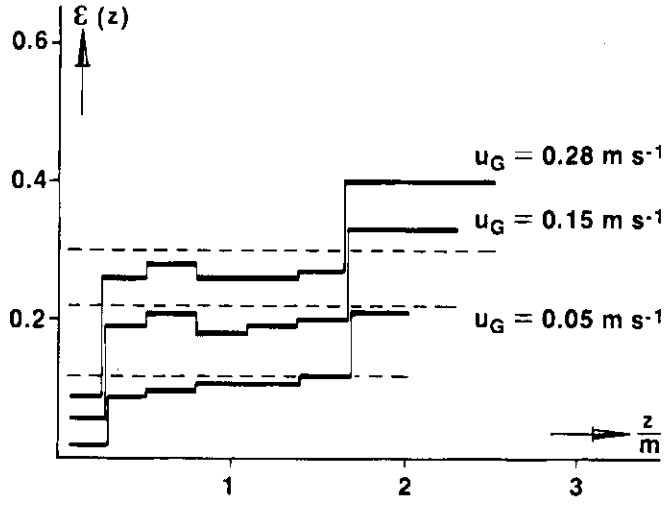

Fig. 2.14. Axial gas holdup distribution for the system air/demineralized water, with H_0 = 1.80 m, for three different superficial gas velocities.

Further experiments were carried out with an electrolyte solution with traces of carbon particles.
The axial gas holdup distribution is given in Fig. 2.17.
It can be seen that the average gas holdup is much higher than that found for the pure electrolyte solution in section 2.5.1. Comparison of the results of Fig. 2.16. and 2.17. shows that traces of carbon particles give a considerable increase of gas holdup.

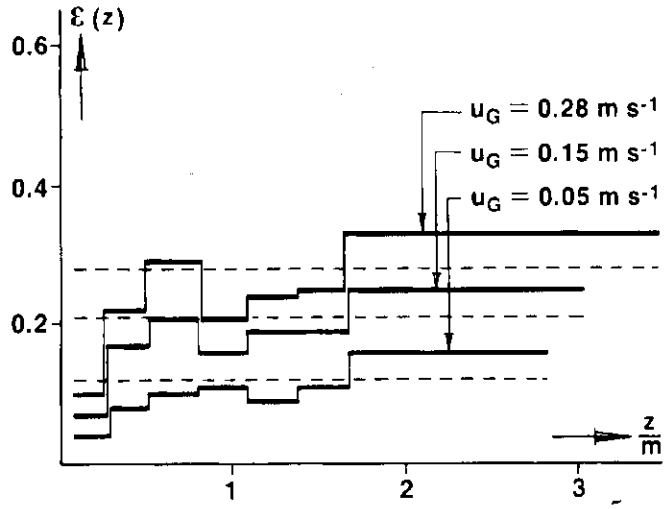

Fig. 2.15. Axial gas holdup distribution for the system air/demineralized water, with H_0 = 2.50 m, for three different superficial gas velocities.

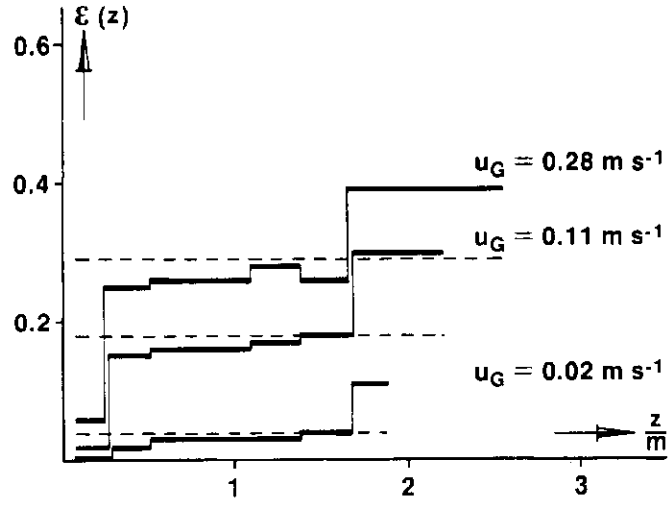

Fig. 2.16. Axial gas holdup distribution for the system air/demineralized water/carbon particles, with $\overline{C}_p$ = 4 kg m^{-3}, for three different superficial gas velocities.

The value of the average gas holdup of the electrolyte solution with traces of carbon particles is identical with the value found in section 2.5.1. for the electrolyte solution containing carbon particles up to a concentration of 8 kg m^{-3}. The distribution pattern agrees with that of the distributions in the above-mentioned systems.

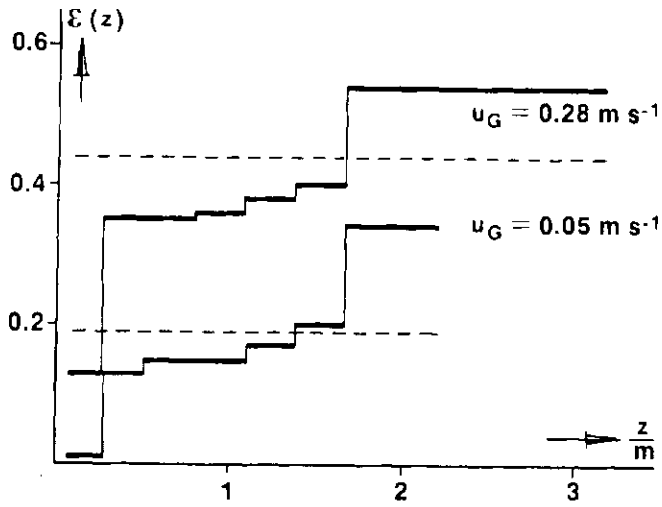

Fig. 2.17. Axial gas holdup distribution for the system air/electrolyte solution containing 23 wt % H_3PO_4 and 17 wt % NH_4NO_3 and traces of carbon particles.

2.5.3. Local solids concentration.
The local solid particle concentration has been measured by taking 25 ml samples of the suspension in the column at seven different heights (7, 27, 51, 80, 109, 138 and 167 cm).
Each sample, taken from the dispersion with a glass tube, was dried at 120 °C for 24 hours. The dry solids were weighed. From these results, the local solids concentration was calculated.
The experiments were performed with the system air/demineralized water with a clear liquid height of 1.80 m and at superficial gas velocities of 0.02, 0.20 and 0.27 m s^{-1}. The average concentrations of carbon particles were 4, 8 and 12 kg m^{-3}.
The concentration of solid particles is expressed by the ratio Ψ:

$$\Psi = C_p(z)/\overline{C}_p \qquad (2\text{-}85)$$

The average concentration of carbon particles $\overline{C}_p$ was calculated from the total mass introduced into the dispersion divided by the liquid volume.
For all measurements Ψ ranged from 0.9 to 1.0.
Moreover, there was no difference in solids concentration between top and bottom of the column.
In Table 2.9., the results of these measurements are given.

Table 2.9. Values of Ψ.

$\overline{C}_p$/(kg m^{-3})	4			8			12		
u_G/(m s^{-1})	Ψ_{mean}	Ψ_{min}	Ψ_{max}	Ψ_{mean}	Ψ_{min}	Ψ_{max}	Ψ_{mean}	Ψ_{min}	Ψ_{max}
0.02	0.9	0.9	1.0	1.0	0.9	1.0	1.0	1.0	1.0
0.20	1.0	0.9	1.0	1.0	1.0	1.0	1.0	1.0	1.0
0.27	1.0	0.9	1.0	1.0	0.9	1.0	1.0	1.0	1.0

From this Table it may be concluded that throughout the dispersion Ψ is 1.0 and that the solid particles were distributed homogeneously.

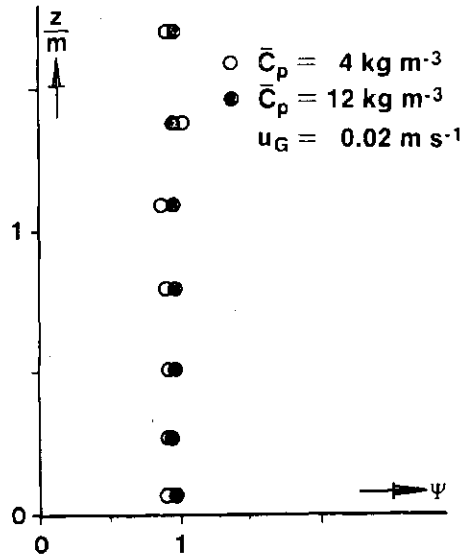

Fig. 2.18. Axial distribution of relative solids concentration in the slurry for u_G = 0.02 m s^{-1} and average solids concentrations of 4 and 12 kg m^{-3}.

2.5.4. Axial liquid-phase velocity distribution.
The liquid-phase velocity distribution was determined at a distance of 167 cm from the bottom of the bubble column. The velocity was calculated from the difference between the static pressure and the dynamic pressure, measured by means of a so-called Prandtl-tube. A drawing of the Prandtl-tube and the corresponding manometer tubes is given in Fig. 2.19.

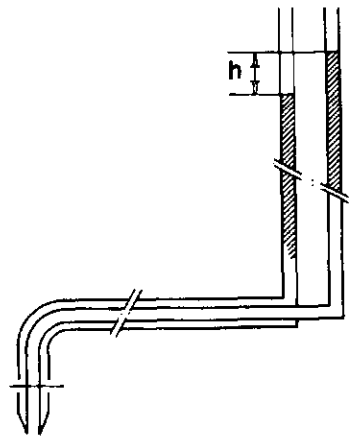

Fig. 2.19. Drawing of the Prandtl-tube and corresponding manometer tubes.

Differences between the static pressure and the dynamic pressure were determined with the Prandtl-tube pointing downwards as well as upwards. From Fig. 2.19., one can deduce that the difference between the dynamic pressure and the static pressure is given by:

$$\tfrac{1}{2}\rho_L \bar{v}_z^2 = h\rho_L g \qquad (2\text{-}86)$$

from which it follows that:

$$\bar{v}_z = (2hg)^{\frac{1}{2}} \qquad (2\text{-}87)$$

The experiments were performed with a clear liquid height of 1.80 m at eight different values of the superficial gas velocity, ranging from 2 to 28 cm s^{-1}. From eqn (2-44), the value of the velocity $\bar{v}_w$ near the wall has been calculated by means of the least-squares method.
In Table 2.10., the values of $\bar{v}_w$ and $\bar{v}_c$ calculated in this way are given.
In Fig. 2.20., the present experimental values are compared with the best-fit curves calculated from eqn (2-44). Up to a superficial gas velocity of about 20 cm s^{-1} the agreement between experimental results and model is good. For higher values of the superficial gas velocity, the agreement is less at r/R = 0.7. Recently, Riquarts [64] proposed a relation for the liquid velocity in the centre of the column:

$$\bar{v}_c = 0.21(gT)^{\frac{1}{2}}\left(u_G^3 \rho_L/(\eta_L g)\right)^{1/8} \qquad (2\text{-}88)$$

In Table 2.10. the experimental velocity near the wall determined with eqn (2-44) is compared with calculated values of the velocity in the centre of the column according to eqn (2-88).
The agreement between the values of $\bar{v}_c$ calculated with the eqns (2-44) and (2-88) is good, particularly at low values of the superficial gas velocity. The difference in values of $\bar{v}_c$ becomes larger with increasing superficial gas velocities.

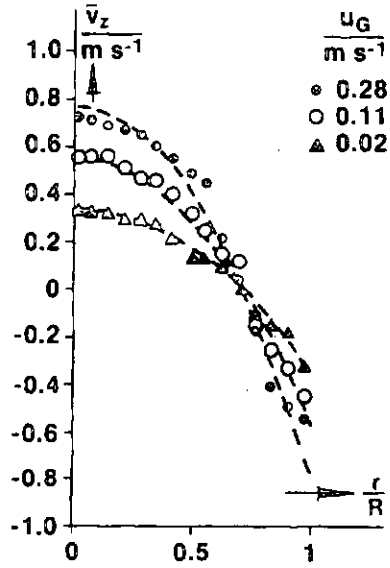

Fig. 2.20. Comparison between experimental values and the best-fit line calculated from eqn (2-44).

Table 2.10. Values of the velocity $\bar{v}_w$ near the wall calculated from eqn (2-44) and comparison of these values with the ones predicted by Riquarts [64].

	present work, eqn (2-44)		Riquarts, eqn (2-88)
$u_G/(m\ s^{-1})$	$\bar{v}_w/(m\ s^{-1})$	$\bar{v}_c/(m\ s^{-1})$	$\bar{v}_c/(m\ s^{-1})$
0.02	-0.36	0.36	0.35
0.05	-0.49	0.49	0.49
0.07	-0.55	0.55	0.55
0.11	-0.60	0.60	0.65
0.15	-0.64	0.64	0.74
0.20	-0.71	0.71	0.82
0.26	-0.76	0.76	0.90
0.28	-0.78	0.78	0.93

2.5.5. Sauter mean gas bubble diameter.

Pictures of the dispersion have been taken by means of a photocamera placed just outside the perspex vessel at a height of 1 m above the bottom of the column. The diaphragm of the lens was 11 and the depth of field was 4 mm.

Each picture showed an area of 24 x 36 mm of the dispersion. A reference tube of 2.00 mm diameter was attached to the inside of the wall.

After development of the film, enlargements were made, in which the bubbles were counted and classified into seven groups. The arithmetic mean bubble diameter of each group was used to calculate the Sauter mean bubble diameter according to eqn (2-50).

This method cannot be used for determining the bubble diameter in sytems containing carbon particles because then no single bubbles can be distinguished.

In this section, the results will be presented for the Sauter mean bubble diameter of the system air/demineralized water with clear liquid heights of 0.74, 1.69 and 2.51 m and of the system air/electrolyte solution with a clear liquid height of 1.78 m.

In Fig. 2.21., the Sauter mean bubble diameter for the air/demineralized water system is given as a function of the superficial gas velocity.

There is almost no difference between the values of d_s for the clear liquid heights of 0.74 m and 1.69 m. In these cases, the Sauter mean bubble diameter is between 3 and 3.5 mm. For the clear liquid height of 2.51 m, the value of the Sauter mean bubble diameter is about 3 mm.

Furthermore, the bubble diameter decreases somewhat with increasing superficial gas velocity. This tendency is identical with that predicted by the correlations mentioned in Table 2.2.

For the system air/demineralized water, the correlation of Mersmann gives a constant value of 4.9 mm for the Sauter mean bubble diameter.

The correlation proposed by Van Dierendonck et al. gives very low values. This phenomenon might be caused by a different specification of the demineralized water used by Van Dierendonck.

Although the correlation of Akita and Yoshida was proposed for $u_G \leq 0.04$ m s^{-1} only, it predicts our experimental values well, even at a superficial gas velocity of about 0.3 m s^{-1}.

Further, we determined the Sauter mean bubble diameter of air in an electrolyte solution containing 17 wt % NH_4NO_3 and 23 wt % H_3PO_4. The experimental values of the mean bubble diameter as a function of the superficial gas velocity are represented in Fig. 2.22. The Sauter mean bubble diameter is between 0.4 and 0.5 mm.

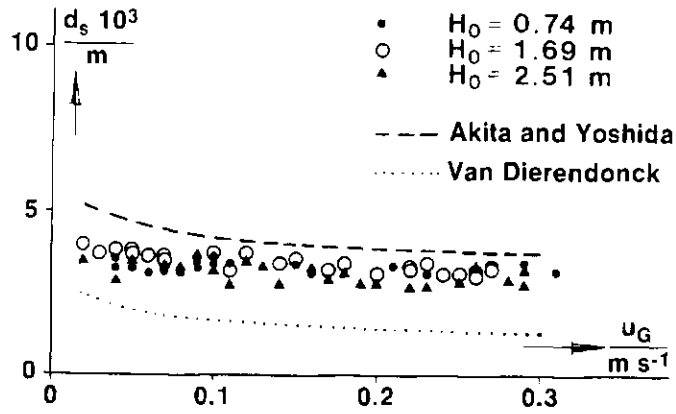

Fig. 2.21. Sauter mean gas bubble diameter for the system air/demineralized water as a function of superficial gas velocity.

The value of the Sauter mean bubble diameter decreases considerably when an electrolyte is added to the pure solvent.
According to the correlation of Mersmann, a value of 4.6 mm is predicted. The values calculated from the correlation of Van Dierendonck et al. show a smaller deviation from our experimental values. It is important to note that the correlation of Van Dierendonck et al. is only valid for $H_0/T < 3$.
De Rooy et al. [11] also found $d_s = 0.5$ mm in an electrolyte-containing aqueous solution for $u_G > 0.05$ m s^{-1}.

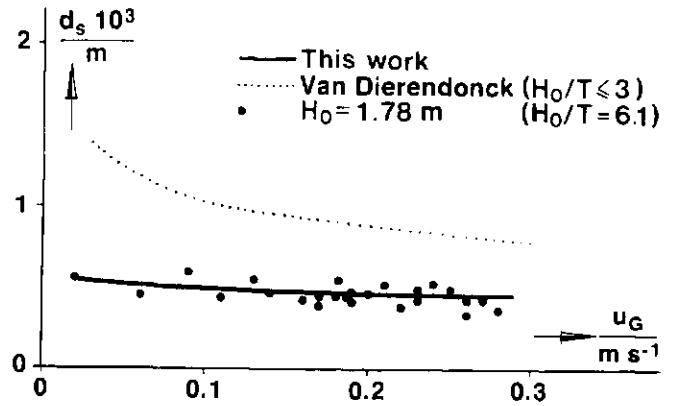

Fig. 2.22. Sauter mean bubble diameter for the system air/electrolyte solution as a function of superficial gas velocity.

2.5.6. Specific interfacial area.
When pictures were taken of the dispersion as described in section 2.5.5., the average gas holdup of the dispersion was measured too, so that the specific interfacial area could be calculated with eqn (2-58).
In Fig. 2.23., experimental values of the specific area for the pure solvent and the values calculated with the correlation of Van Dierendonck (eqn (2-59)) are plotted versus the superficial gas velocity.
Combination of eqns (2-6) and (2-58) results in:

$$a = 6u_G\{(v_o + bu_G)d_s\}^{-1} \qquad (2\text{-}89)$$

Substitution of v_o = 0.35 m s^{-1}, b = 2 and d_s = 3.3 mm leads to the solid curve in Fig. 2.23.

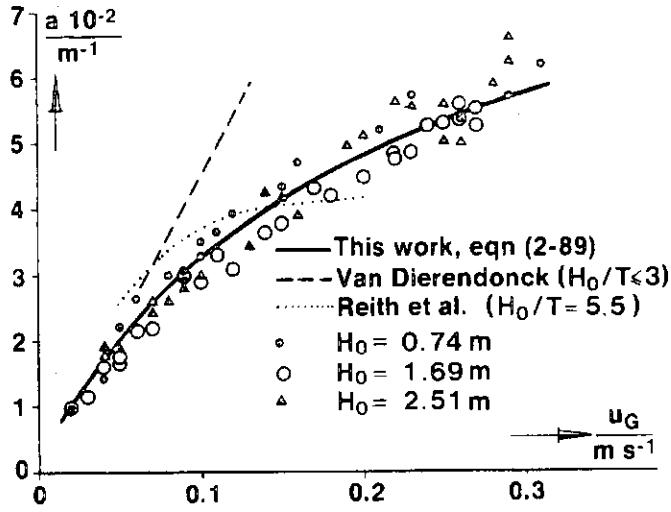

Fig. 2.23. Specific interfacial area for the system air/demineralized water as a function of superficial gas velocity.

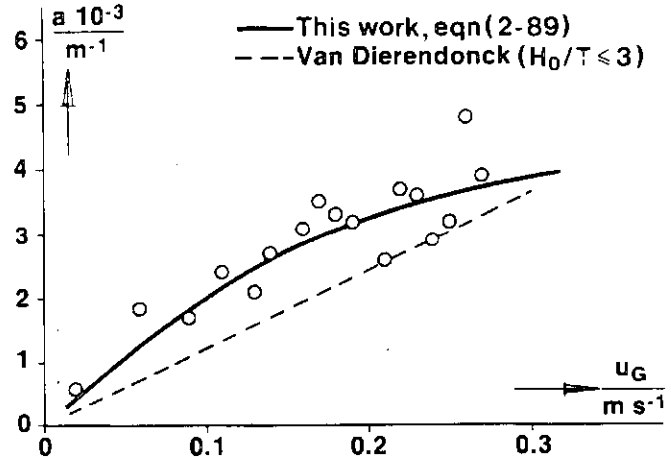

Fig. 2.24. Specific interfacial area for the system air/electrolyte solution as a function of superficial gas velocity.

Our experimental values for the system air/demineralized water are much lower than those predicted by the correlation of Van Dierendonck et al. This is probably due to the much smaller bubble diameter as well as the higher average gas holdup which were found by Van Dierendonck. Our results with demineralized water agree with the experimental data given in the work of Reith et al. [41] for $u_G < 0.2$ m s^{-1} and $H_0/T = 5.5$ with $T = 0.29$ m.
In Fig. 2.24., the experimental values of the specific area for the system air/electrolyte solution and the values calculated with Van Dierendonck's correlation (eqn (2-59)) are plotted versus the superficial gas velocity. Substitution of $v_o = 0.46$ m s^{-1}, $b = 1.87$ and $d_s = 0.45$ mm leads to the solid curve in Fig. 2.24.

2.5.7. Dynamic gas disengagement.
In this section, the results of the dynamic gas-disengagement experiments are presented. These experiments were performed with four different systems:
(a)- air/demineralized water (H_0/T values of 3.4, 6.0 and 8.5);
(b)- air/demineralized water/carbon particles ($H_0/T \approx 6$ and $\overline{C}_p$ values of 4, 8 and 12 kg m^{-3});
(c)- air/electrolyte solution ($H_0/T \approx 6$);
(d)- air/electrolyte solution/carbon particles ($H_0/T \approx 6$ and $\overline{C}_p \approx 4$ kg m^{-3}).

For the systems (a) and (c), the experimental values of both the Sauter mean bubble diameter and the specific interfacial area obtained from dynamic gas-disengagement experiments were compared with the results from pictures of the dispersion (see sections 2.5.5. and 2.5.6.).
In Fig. 2.25., the experimental set up is shown.
In the bubble column, a float A swims in the upper layer of the gas-liquid dispersion. The float is guided by two vertical ropes B_1 and B_2 so that it can only move along its vertical axis and horizontal movement is excluded.

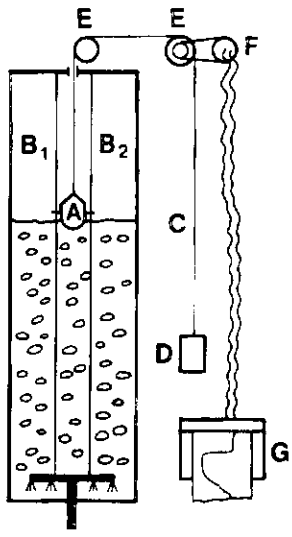

Fig. 2.25. Experimental set up for the gas-disengagement experiments.
A. float
B_1 and B_2. ropes
C. chain
D. counterweight
E. chain-wheels
F. potentiometer
G. recorder

The float is connected by means of a chain C with a counterweight D outside the column.
At the top of the bubble column the chain drives a chain-wheel E. The chain-wheel turns a potentiometer by means of a gearbox with three different transmission ratios.
Depending on the height of the collapse, the correct transmission ratio was chosen to make use of the complete range of the potentiometer.
With the potentiometer a signal was sent to a recorder on which a curve was drawn representing the height of the dispersion as a function of time.
Eqn (2-73) can be approximated by:

$$(H(t') - H_0)/\varepsilon_{av} = H(t')\sum_{0}^{v(t')} f_1(w)\Delta w - t'\sum_{0}^{v(t')} w f_1(w)\Delta w \qquad (2\text{-}90)$$

In Fig. 2.26., a typical experimental gas-disengagement curve is shown.
We found that the float falls about 30 % of the height $H_D - H_0$ within two seconds after cut-off of the gas supply.

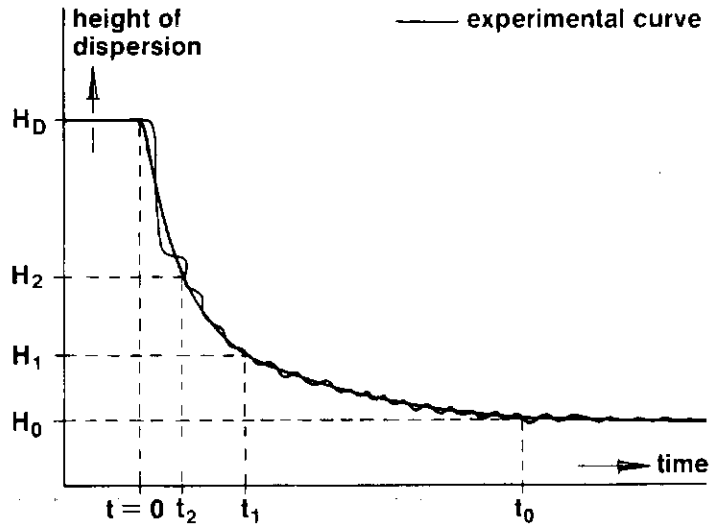

Fig. 2.26. Typical gas-disengagement curve, showing the height of the dispersion as a function of time.

From this curve it can be deduced that:

$$(H_1 - H_0)/\varepsilon_{av} = H_1 f_1(v_0)\Delta w - t_1 v_0 f_1(v_0)\Delta w \qquad (2\text{-}91)$$

Rearranging of eqn (2-91) and substitution of $v_0 = H_0/t_0$ gives:

$$f_1(v_0)\Delta w = \frac{H_1 - H_0}{\varepsilon_{av}} \frac{t_0}{H_1 t_0 - H_0 t_1} \qquad (2\text{-}92)$$

Further, it can be found from Fig. 2.26. that:

$$(H_2 - H_0)/\varepsilon_{av} = H_2\{f_1(v_0)\Delta w + f_1(v_1)\Delta w\} - t_2\{v_0 f_1(v_0)\Delta w + v_1 f_1(v_1)\Delta w\} \qquad (2\text{-}93)$$

Rearranging of eqn (2-93) and substitution of $v_1 = H_1/t_1$ gives:

$$f_1(v_1)\Delta w = \frac{(H_2 - H_0)/\varepsilon_{av} - H_2 f_1(v_0)\Delta w + t_2 H_0 f_1(v_0)\Delta w/t_0}{H_2 - t_2 H_1/t_1} \qquad (2\text{-}94)$$

In general, eqn (2-94) reads:

$$f_1(v_i)\Delta w = \frac{(H_{i+1} - H_0)/\varepsilon_{av} - H_{i+1}\sum_0^{v_{i-1}} f_1(w)\Delta w + t_{i+1}\sum_0^{v_{i-1}} w f_1(w)\Delta w}{H_{i+1} - t_{i+1}H_1/t_1} \qquad (2\text{-}95)$$

in which:

$$v_{i-1} = H_{i-1}/t_{i-1} \qquad (2\text{-}96)$$

With eqns (2-92) and (2-95) we are able to find a volume fraction distribution as a function of the velocity of rise of the gas bubbles.
In Fig. 2.27., a typical histogram is drawn.

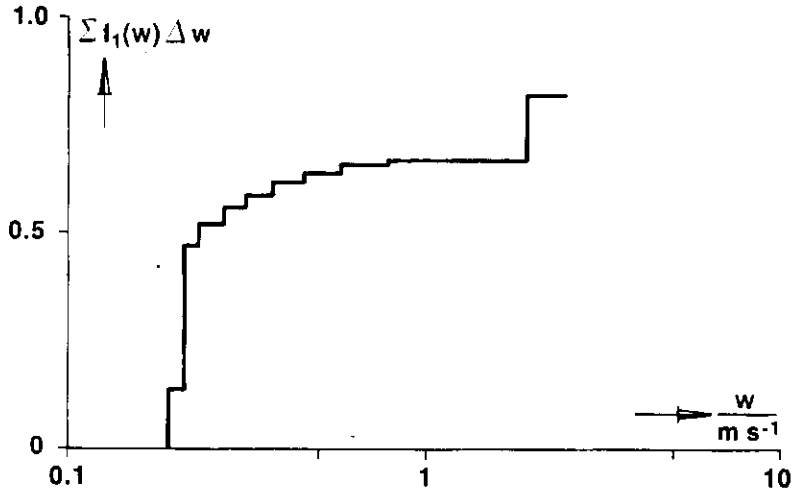

Fig. 2.27. Typical gas-disengagement histogram, showing the volume fraction distribution as a function of the velocity of rise of the gas bubbles (system air/demineralized water, $H_0/T = 8.6$, $u_G = 0.26$ m s^{-1}, $\varepsilon_{av} = 0.25$).

For calculation of the Sauter mean diameter and the specific interfacial area, it is necessary to transform the volume distribution as a function of the velocity of rise into a volume distribution as a function of gas bubble diameter.
We used the relation describing the correlation between diameter and terminal velocity of rise:

$$\pi d_b^3 \Delta\rho g/6 = C_w \pi d_b^2 \rho_L v_o^2/8 \qquad (2\text{-}97)$$

with:

$$C_w = 18.5/Re_b^{0.6} \text{ for } Re_b < 500 \qquad (2\text{-}98)$$

and:

$$C_w = 0.44 \text{ for } Re_b \geq 500 \qquad (2\text{-}99)$$

From the eqns (2-97), (2-98) and (2-99), we find that:

$$d_b = \{13.875\ \nu_L^{0.6} v_o^{1.4}/g\}^{0.625} \text{ for } Re_b \leq 500 \qquad (2\text{-}100)$$

and:

$$d_b = 0.33\ v_o^2/g \text{ for } Re_b \geq 500 \qquad (2\text{-}101)$$

The value $Re_b = 500$ for the system air/demineralized water corresponds with a velocity of rise of 0.25 m s^{-1} or a bubble diameter of 2 mm.
In Fig. 2.28., we present a typical histogram as a function of the gas bubble diameter.

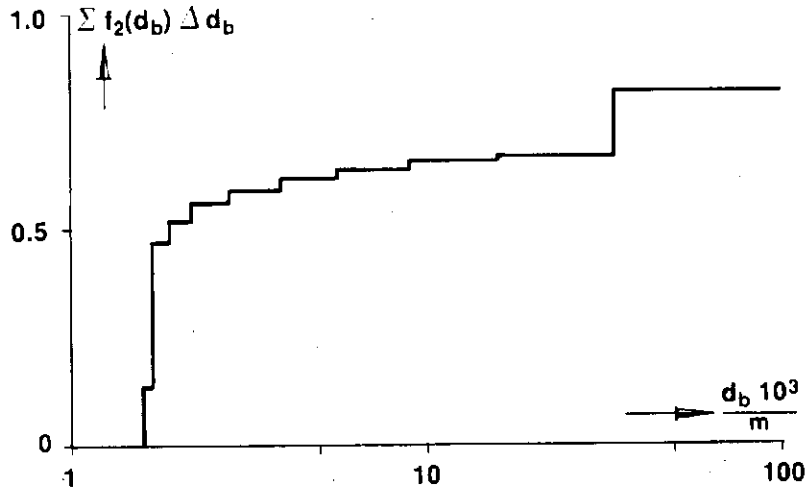

Fig. 2.28. Typical gas-disengagement histogram, showing the volume fraction distribution as a function of the gas bubble diameter (system air/demineralized water, $H_0/T \simeq 8.6$, $u_G = 0.26$ m s^{-1}, $\varepsilon_{av} = 0.25$).

The Sauter mean bubble diameter is given by:

$$d_s = \sum_i n_i d_i^3 / \sum_i n_i d_i^2 \qquad (2\text{-}102)$$

in which d_i is the arithmetic mean diameter of a bubble of class i.
The number of bubbles in class i is found from:

$$n_i = 6(f_2(d_b)\Delta d_b)_i V_G/(\pi d_i^3) \qquad (2\text{-}103)$$

Substitution of eqn (2-103) into eqn (2-102) yields:

$$d_s = \sum_i (f_2(d_b)\Delta d_b)_i / \{\sum_i ((f_2(d_b)\Delta d_b)_i/d_i)\} = \{\sum_i ((f_2(d_b)\Delta d_b)_i/d_i)\}^{-1} \qquad (2\text{-}104)$$

Finally, the specific interfacial area can be calculated from:

$$a = 6\varepsilon_{av}/d_s \qquad (2\text{-}105)$$

It should be pointed out that all calculations presented in this section are performed under the restriction that:
- the correlation between bubble diameter and terminal velocity of rise is given by eqn (2-97);
- only the volume fraction of those bubbles whose diameter is smaller than that calculated from eqn (2-52) is taken into account. For the systems (a) and (b) this implies $d_b \leq 8$ mm and $v_o \leq 0.49$ m s^{-1}.

First, we have performed gas-disengagement experiments with the system air/demineralized water with clear liquid heights of 0.98, 1.75 and 2.46 m. In Figs. 2.29., 2.30. and 2.31., the experimental values of the Sauter mean bubble diameter are drawn. In these figures, the experimental data for the Sauter mean bubble diameter as obtained from pictures of the dispersion and discussed in section 2.3.5. are given too. The figures show that there is a good agreement for the bubble diameter obtained from both methods for clear liquid heights of 1.75 and 2.46 m. For a clear liquid height of 0.98 m, the results of both methods differ by about 10 - 20 %.

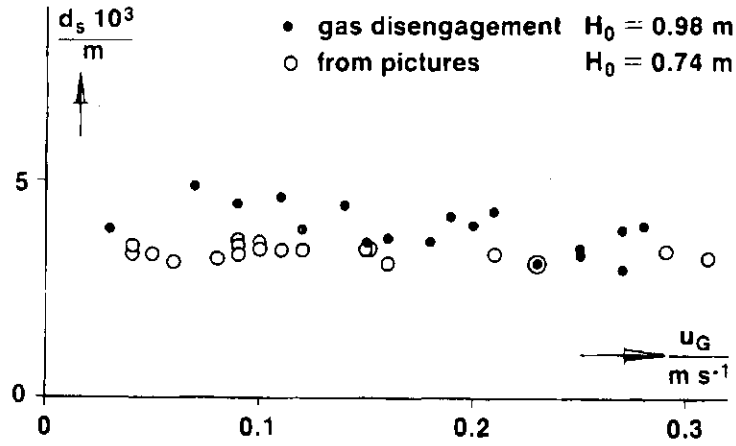

Fig. 2.29. Experimental values of the Sauter mean bubble diameter as a function of the superficial gas velocity for the system air/demineralized water, $H_0/T \simeq 3$.

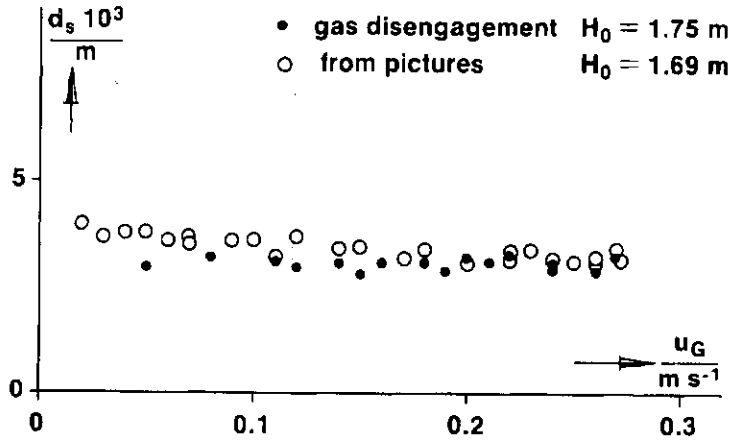

Fig. 2.30. Experimental values of the Sauter mean bubble diameter as a function of the superficial gas velocity for the system air/demineralized water, $H_0/T \simeq 6$.

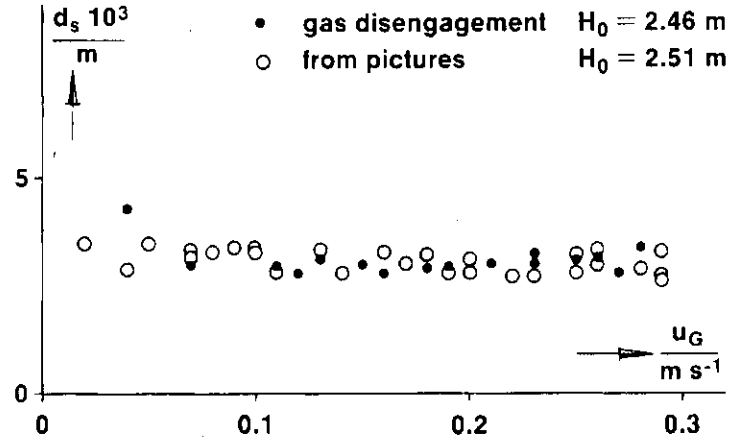

Fig. 2.31. Experimental values of the Sauter mean bubble diameter as a function of the superficial gas velocity for the system air/demineralized water, $H_0/T \approx 8.6$.

In Figs. 2.32., 2.33. and 2.34., the experimental values of the specific interfacial area are given for both methods.

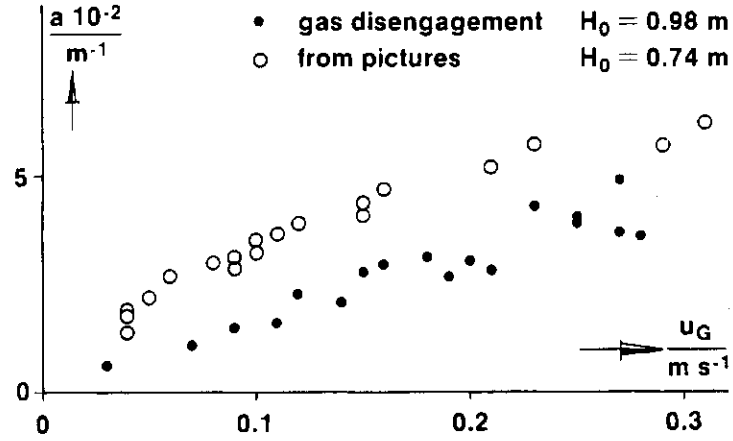

Fig. 2.32. Experimental values of the specific interfacial area as a function of the superficial gas velocity for the system air/demineralized water, $H_0/T \approx 3$.

The values of the specific interfacial area obtained from the pictures are somewhat higher than those from the gas-disengagement experiments. This difference is due to the difference in gas holdup value used. For calculating the specific interfacial area from the pictures, we used the visually observed height of the dispersion, so including a small region near the level of the dispersion with a relatively high gas holdup.
In the case of the gas-disengagement experiments, we made use of the height of the dispersion, excluding the small foam layer, determined graphically by means of the float.

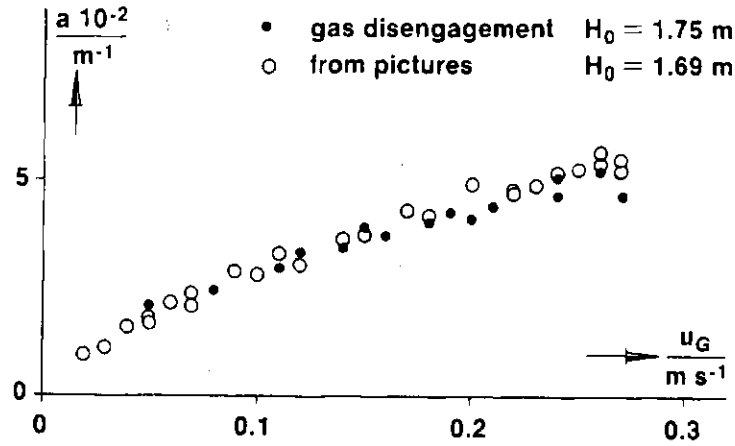

Fig. 2.33. Experimental values of the specific interfacial area as a function of the superficial gas velocity for the system air/demineralized water, $H_0/T = 6$.

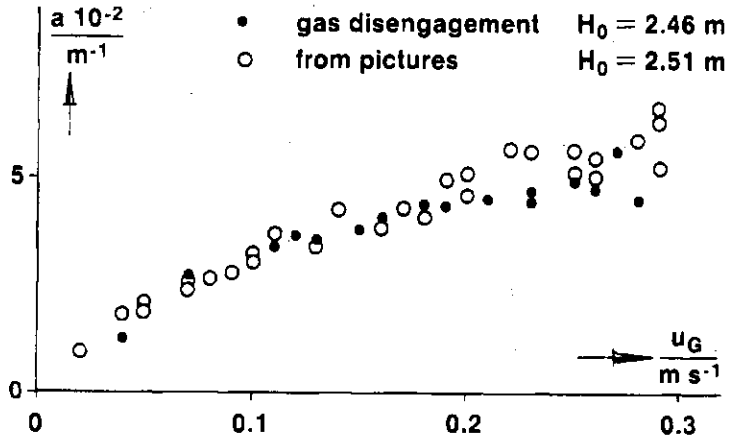

Fig. 2.34. Experimental values of the specific interfacial area as a function of the superficial gas velocity for the system air/demineralized water, $H_0/T \approx 8.5$.

Further experiments were carried out with a clear liquid height of about 1.7 - 1.8 m with the system air/demineralized water/carbon particles. The concentration of solid particles in the liquid was 4, 8 and 12 kg m^{-3}. In Fig. 2.35., we compare the values of the Sauter mean bubble diameter for three different concentrations of carbon particles. For the sake of clarity, the values for a solid concentration of 8 kg m^{-3} have been omitted. It is obvious that there is no difference in Sauter mean bubble diameter for the three different solids concentrations, which means that addition of carbon particles to the system air/demineralized water does not influence the value of the gas bubble diameter. In Fig. 2.36., the values of the specific interfacial area are compared.

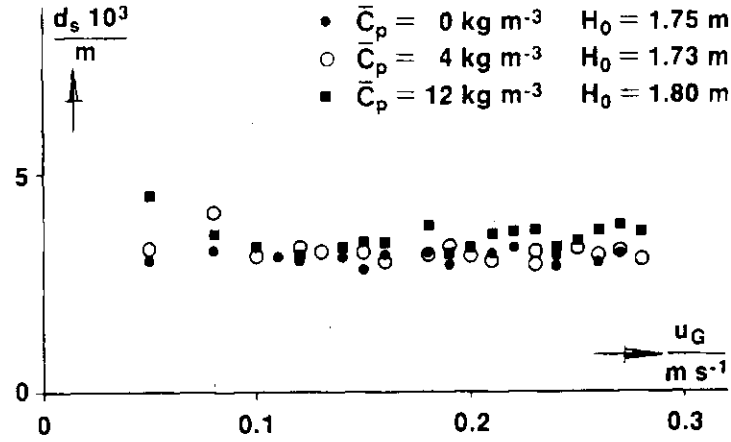

Fig. 2.35. Experimental values of the Sauter mean bubble diameter as a function of the superficial gas velocity for the system air/demineralized water/carbon particles, $H_0/T \approx 6$.

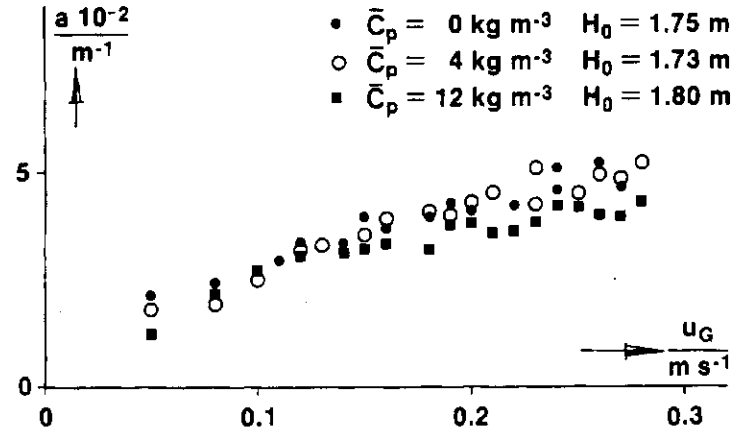

Fig. 2.36. Experimental values of the specific interfacial area as a function of the superficial gas velocity for the system air/demineralized water/carbon particles, $H_0/T \approx 6$.

The value of the specific interfacial area for the system with a solids concentration of 12 kg m^{-3} tends to be somewhat smaller than that for the other concentrations.

Further experiments were performed with the system air/electrolyte solution with and without carbon particles. The concentration of solid particles was 4 kg m^{-3}.
In Fig. 2.37., the values of the Sauter mean bubble diameter are given for the different systems investigated.
It is obvious that there is a large difference between the values obtained from pictures and those calculated from the gas-disengagement experiments.
From Fig. 2.37., the conclusion can be drawn that for the system air/electrolyte

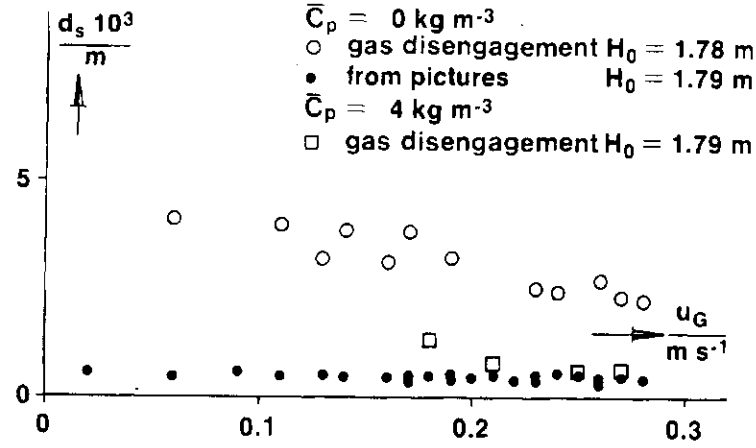

Fig. 2.37. Experimental values of the Sauter mean bubble diameter as a function of the superficial gas velocity for the system air/electrolyte solution with and without carbon particles, $H_0/T \approx 6$.

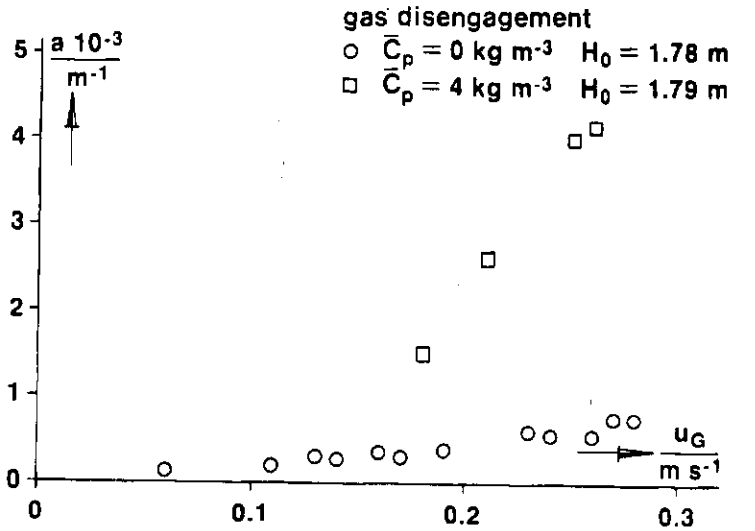

Fig. 2.38. Experimental values of the specific interfacial area as a function of the superficial gas velocity for the system air/electrolyte solution with and without carbon particles, $H_0/T \approx 6$.

solution the value of the Sauter mean bubble diameter obtained from gas-disengagement experiments is much higher than the values of d_s obtained from pictures. This value of d_s obtained from gas-disengagement experiments is about the same as for the system air/demineralized water with and without carbon particles.

This difference could be caused by the following:

- pictures taken from outside the bubble column represent only a small layer of the dispersion just near the wall of the column. This layer may not be representative of the bubble size distribution, which may result in too small a calculated value of d_s.
- the decrease of the height of the dispersion per unit of time at the end of

the gas-disengagement experiment is small. This causes relatively large errors in the calculated values of the volume fraction and the bubble diameter.

When carbon particles were added to the electrolyte solution, the value of the Sauter mean bubble diameter obtained from gas-disengagement experiments was about the same as the value of d_s for the system air/electrolyte solution without carbon particles as obtained from pictures.

In Fig. 2.38., the corresponding values of the specific interfacial area are given.

2.6. Summary and conclusions.

In this chapter, experimental values for the average gas holdup, the gas-holdup distribution, the solids concentration distribution, the axial liquid-velocity distribution, the Sauter mean bubble diameter and specific interfacial area of both a bubble column and a slurry column have been given. The experimental results have been compared with correlations proposed in the literature.

With respect to the average gas holdup, we may conclude that:

- our experimental results are in agreement with relations found in the literature for the system air/demineralized water as well as for the system air/electrolyte solution;
- addition of electrolytes or carbon particles to demineralized water does not influence the value of the average gas holdup as long as the superficial gas velocity remains the same;
- the correlation between average gas holdup in aqueous solutions and superficial gas velocity can be represented by

$$\varepsilon_{av} = u_G/(v_o + bu_G) \qquad (2\text{-}106)$$

  with $b \approx 2$ and $v_o \approx 0.35$ m s^{-1};
- addition of both carbon particles and electrolyte to demineralized water increases the average gas holdup to about 0.5 for $u_G > 0.1$ m s^{-1} and causes the formation of a foam layer whose height decreases with increasing superficial gas velocity;
- the clear liquid height influences the value of the average gas holdup only slightly provided that $H_0/T > 3$.

With respect to the gas holdup distribution, it was found that:

- for the major part of the dispersion (middle section, see Fig. 2.1.), the gas holdup is lower than the average gas holdup;
- the local gas holdup increases in the direction from the bottom to the top of the dispersion;
- the gas holdup near the sparger is lower than the average gas holdup;
- in the foam layer the gas holdup has a much higher value than the average one;
- qualitatively, there is no difference between the various aqueous systems as to the axial gas holdup distribution patterns.

With respect to the solid carbon particle concentration ($d_p < 30$ μm), we may conclude that:

- the concentration of solid carbon particles is constant throughout the dispersion and deviates by less than 10 % from the mean solids concentration even at a superficial gas velocity as low as 2 cm s^{-1}.

In section 2.2.4., it was shown that:

- the axial liquid velocity in the dispersion can be approximated by:

$$\bar{v}_z(r) = 2\bar{v}_w\{(r/R)^2 - \tfrac{1}{2}\} \qquad (2\text{-}107)$$

- both literature data and experimental results of the present work are in good agreement with eqn (2-107);
- for $u_G > 0.2$ m s^{-1}, the experimental values of the local liquid velocity for $r/R \approx 0.7$ slightly deviate from the best-fit values;
- the liquid velocity in the centre of the dispersion is in good agreement with values calculated from the prediction equation (2-88) from the literature [64].

With respect to the Sauter mean bubble diameter, it can be noted that for the system air/demineralized water:
- the value of d_s was between 3 and 3.5 mm and decreased slightly with increasing superficial gas velocities;
- our experimental values of d_s were somewhat smaller than the values predicted by the correlation of Akita and Yoshida;
- the correlation of Van Dierendonck et al. gives too low values for d_s for this system, probably due to a different specification of "demineralized water".

With respect to the Sauter mean bubble diameter, it can be noted that for the system air/electrolyte solution:
- the value of d_s was between 0.4 and 0.5 mm and almost constant;
- our experimental values of d_s were smaller than the values predicted by the correlation of Van Dierendonck et al.

With respect to the specific interfacial area, it can be concluded that:
- for the system air/demineralized water, our experimental values of a_L were in agreement with the experimental values of Reith et al. but not with those of Van Dierendonck et al.;
- for the system air/electrolyte solution, our experimental values of a_L were in agreement with the values predicted by the correlation of Van Dierendonck et al.

With respect to the experimental results of the gas-disengagement experiments for determining d_s and a_L, it was found that:
- for the system air/demineralized water, the values of d_s and a_L were in good agreement with those obtained from the pictures;
- addition of carbon particles to the system air/demineralized water did not influence the value of d_s or a_L;
- for the system air/electrolyte solution, the experimental values of d_s and a_L were of the same order of magnitude as for the system air/demineralized water with and without carbon particles and differed from those of the pictures of the system air/electrolyte solution without carbon particles.